scientific reports

Check for updates

OPEN

The cranium from the Octagon in Ephesos

Gerhard W. Weber[1,2]✉, Petra G. Šimková[1,2], Daniel M. Fernandes[2,3], Olivia Cheronet[1,2], Előd Úry[1,2], Harald Wilfing[1,2], Katarina Matiasek[1,2], Alejandro Llano-Lizcano[1,2], Pere Gelabert[1,2], Immo Trinks[2,4], Katerina Douka[1,2], Sabine Ladstätter[2,5,6], Tom Higham[1,2], Martin Steskal[2,5] & Ron Pinhasi[1,2]

During excavations in 1929, a well-preserved skeleton was discovered in a sarcophagus in the Octagon at Ephesos (Turkey). For the following century, archaeologists have speculated about the identity of this obviously notable person. Repeated claim is that the remains could represent Arsinoë IV, daughter of Ptolemy XII, and younger (half-)sister of Cleopatra VII. To address these questions we undertook state-of-the-art morphological, genetic and dating analyses of the cranium and further analyses of bone samples from a femur and a rib of the skeleton found in the same tomb. We confirm based on genetic analyses from the cranium and the femur that they derive from the same person. ^{14}C-dating of the cranium provides a most likely time range between 205–36 BC. The connection with Arsinoë IV can be excluded because we confirmed that the individual is a male. The cranium represents an 11-14-year-old boy who suffered from significant developmental disturbances. Genetics suggest an ancestry from the Italian peninsula or Sardinia. The fate of the body of Arsinoë IV, who reportedly was killed in 41 BC in Ephesos, remains open. In contrast, investigations regarding the fate and social background of the boy from the Octagon can now proceed free of speculation.

Keywords Arsinoë IV, Ptolemean, Ephesos, Cranial morphology, Ancient DNA

The history of archaeological excavations at the ancient city of Ephesos goes back more than 100 years. The site represents one of the most important ancient localities in Asia Minor. The Austrian Archaeological Institute has been active there since 1895[1]. In 1904, Rudolf Heberdey, Josef Keil and Wilhelm Wilberg uncovered the Octagon and other buildings along the lower "Kuretenstraße" in the city centre of ancient Ephesos[2]. Due to its architecture and important location, the Octagon was immediately considered a heroon upon discovery. It took until 1929 that Max Theuer and Josef Keil were able to open the burial chamber of the Octagon in a further excavation and discovered a marble sarcophagus. No grave goods or inscriptions were found in the chamber or on the sarcophagus to hint at the identity of the deceased. The sarcophagus was almost completely filled with water but revealed a single skeleton at its bottom[3]. For an unknown reason, Keil only removed the cranium from the tomb, which was then closed again. The post-cranial remains stayed in the burial chamber, along with, likely, the mandible. We know with certainty that Keil[3] took the cranium back to Greifswald (Germany) where he was a professor of ancient history. After investigating it, he immediately speculated about "the possibly very distinguished personality" of the individual who was interpreted as being about 20 years old, and likely a female. Keil did not provide any data, only his and his colleague's opinions, but he prepared the way for further speculations[4].

The architectural style of the Octagon was subsequently recognized to resemble the Pharos of Alexandria[2], although there are also substantial opinions that argue against an identification as Pharos[4]. The tentative construction date might come close to the last decades BC[5,6]. Building upon the particular structural shape suggesting possible Egyptian influence, the remarkable prominence of the Octagon within the Ephesos urban area, and upon Keil's anthropological assessment that the person buried in the Octagon was a 20-year-old female, Hilke Thür[2] formulated her hypothesis that the buried person could be Arsinoë IV. She was one of the five children of King Ptolemy XII who ruled the Ptolemaic Kingdom of Egypt from 80 to 51 BC[7]. Arsinoë IV is not only historically important as the (half-)sister of Cleopatra VII, but also because she conducted the siege of Alexandria in 48 – 47 BC against Cleopatra VII, who allied with the Roman emperor Julius Caesar. Arsinoë IV

[1]Department of Evolutionary Anthropology, University of Vienna, Djerassiplatz 1, A-1030 Vienna, Austria. [2]Human Evolution and Archaeological Science (HEAS), University of Vienna, Vienna, Austria. [3]Department of Life Sciences, CIAS, University of Coimbra, 3000-456 Coimbra, Portugal. [4]Vienna Institute for Archaeological Science (VIAS), University of Vienna, Vienna, Austria. [5]Austrian Archaeological Institute, Austrian Academy of Sciences, Vienna, Austria. [6]Sabine Ladstätter is deceased. ✉email: gerhard.weber@univie.ac.at

lost this battle, was captured, and exhibited in chains in Rome in 46 BC. She was described as scared and weeping but no distinctive features in her appearance were noted in Rome[8]. She was then protected in the asylum of the Temple of Artemis in Ephesos. A few years later Cleopatra VII allied with Marcus Antonius who reportedly[9,10] gave the order to execute Arsinoë IV in 41 BC.

As Josef Keil became a professor of Greek and ancient history at the University of Vienna (1936 to 1950), the cranium from the Ephesos Octagon moved with Keil to his department at the University of Vienna[4]. Josef Weninger, who led the Anthropological Institute in Vienna until 1955, published a paper on the morphology of the cranium in 1953[11]. In addition to the classical craniometric measurements, Weninger determined the age at death between 16 and 17 years, and female sex. Weninger[11] described the development of the cranium as undisturbed and did not mention any abnormalities other than minor tooth wear, a cranium of reduced height with almost missing canine fossae, absent incisura malaris and strongly skewed mandibular articulation, and a reduced maxillary body. He further speculated about a "refined type of human" which could point to higher aristocracy. With this description, he further fuelled hypotheses towards the skeleton belonging to Arsinoë IV. The cranium sank into oblivion and remained unregarded until December 2022[4]. Comparing the cranium with the label "Ephesos Heroengrab" [translation: Ephesos Heroon] marked on its occipital bone with the images in Weninger's 1953 publication[11], it became certain that this was indeed the cranium that Keil had recovered from the Octagon sarcophagus and had taken to Vienna[4].

Less certain is the fate of the post-cranial remains. In 1982, the Octagon was re-visited under the direction of Hermann Vetters and the grave-chamber was re-opened[4]. The post-cranium was discovered in two niches of the chamber's northern wall, and several bones above the lintel at the inner end of the Dromos (an entrance passage leading to a tomb)[4]. If this was indeed the postcranial skeleton that J. Keil had seen in the watered sarcophagus in 1929[3], we can only speculate when and how it got out of the sarcophagus, since no reports are available regarding this question. In 1993, Hilke Thür re-entered the tomb and initiated an examination of these postcranial remains. Finally, in 2007, some more pieces of the postcranium were found in the Dromos[12,13], among them a rib fragment. Due to the absence of a continuous and conclusive history, the postcranial remains and the cranium had to be treated as separate individuals until the opposite was proven. Kanz and colleagues released a conference poster on morphological and pathological analysis of the post-cranium from the Octagon in 2009[12], including a soft tissue reconstruction of the unconfirmed Arsinoë IV cranium, even though the cranium was neither physically nor virtually accessible at that time, except from the few images that Weninger published in 1953[11]. Kanz and colleagues[12] estimated the age at death between 15 and 17 years, reconstructed a body height of 154 cm (± 3 cm), and suggested the skeleton was female. According to these authors, the skeleton appeared slim and fragile and showed no stress markers or signs of heavy labour. A radiocarbon date they obtained yielded a date range between 210 and 20 BC (94% prob.), and their DNA analyses did not conclusively reveal any significant data.

Results

The morphology of the Octagon-Cranium

The Octagon-cranium is well preserved (Fig. 1), showing only two larger post-mortal defects in the left and right temporal regions, and missing outer alveolar rims from the upper left first molar (M^1) to the third molar (M^3), as well as from the upper right premolar (P^3) to the M^3. Only the upper left P^3 and upper left M^1 are in situ; the other teeth described by Weninger[11] (upper right M^1 and M^2, upper left M^2, lower right M_1) are missing and could not be found in the collection of the Department of Evolutionary Anthropology at the University of Vienna. The mandible is missing and was never mentioned, neither by Keil[3] nor by Weninger[11], although Weninger listed a lower right molar which raises the question of its misclassification. The cranium is fragile, cranial bones are thin, and muscle markers are weak, traits that are compatible with either a female status (which Weninger proposed) or an adolescent male status. The cranium appears brachycranic (short and broad), and low in relation to length (chamaecranic) and width (hyper-tapeinocranic). Selected traditional craniometric measurements are provided in Table 1 in comparison to the values of Weninger[11]. Weninger, however, described the cranium as the opposite, namely dolichocranic[11], p. 167]. The virtual endocast shows an endocranial capacity of 1428.75 cm^3 which is within the usual range of modern humans, and a right occipital and a weak left frontal petalia, which are opposite to the dominant pattern in humans[14] (Supplementary Information Fig. S6).

Conspicuous are strong signs of asymmetry and deformations that were not described before. In basal view, the whole cranium shows a flexion. The occiput is displaced to the left, and the foramen magnum is oriented obliquely. Both occipital condyles, despite the young age of the individual (see below), show severe pre-mortal defects on the medial and anterior rims of the articulation surfaces (Supplementary Information Fig. S7). The deep mandibular fossae are unremarkable but show an extreme angulation to the midsagittal plane (MSP) of the cranium (Figs. 1f and 2). Left and right sides in addition differ notably by ~ 3 degrees (axial condylar angle left 48.3°, right 51.5°). In a recent sample of 64 symmetric and asymmetric patients from Taiwan, the axial condylar angle was found to be 74.97° (± 6.43° S.D.) for symmetric, respectively 74.04° (± 8.71° S.D.) for asymmetric patients[15], putting the Octagon cranium outside 3 S.D.s of the symmetric and just within 3 S.D.s of the asymmetric sample. In a study of 82 individuals from Brazil[16], the mean inclination of the mandibular condylar process was found to be 65.03° right (± 9.05° S.D.) and 63.44° left (± 7.90° S.D.). The left-right difference is half of that of the Octagon-cranium, and the difference in angle, compared to the Taiwanese sample, is smaller, thus the Octagon-cranium is within − 1.5 S.D. for the right and − 1.9 S.D. for the left side. A further study from Turkey[17] reports a horizontal condylar angle of 25.68° (± 9.31° S.D.), corresponding to 64.32° (± 9.31° S.D.) axial condylar angle for 31 healthy control individuals which is very similar to[16]. High-resolution µCT-scans (80 µm) of the inner ear (taken before genetic sampling, see Methods) reveal average size and shape of the preserved auditory ossicles, represented only by the left malleus and the right incus. Whether the other ossicles got lost in the course of the last two millennia or their absence is associated with ossicular chain deformities remains open.

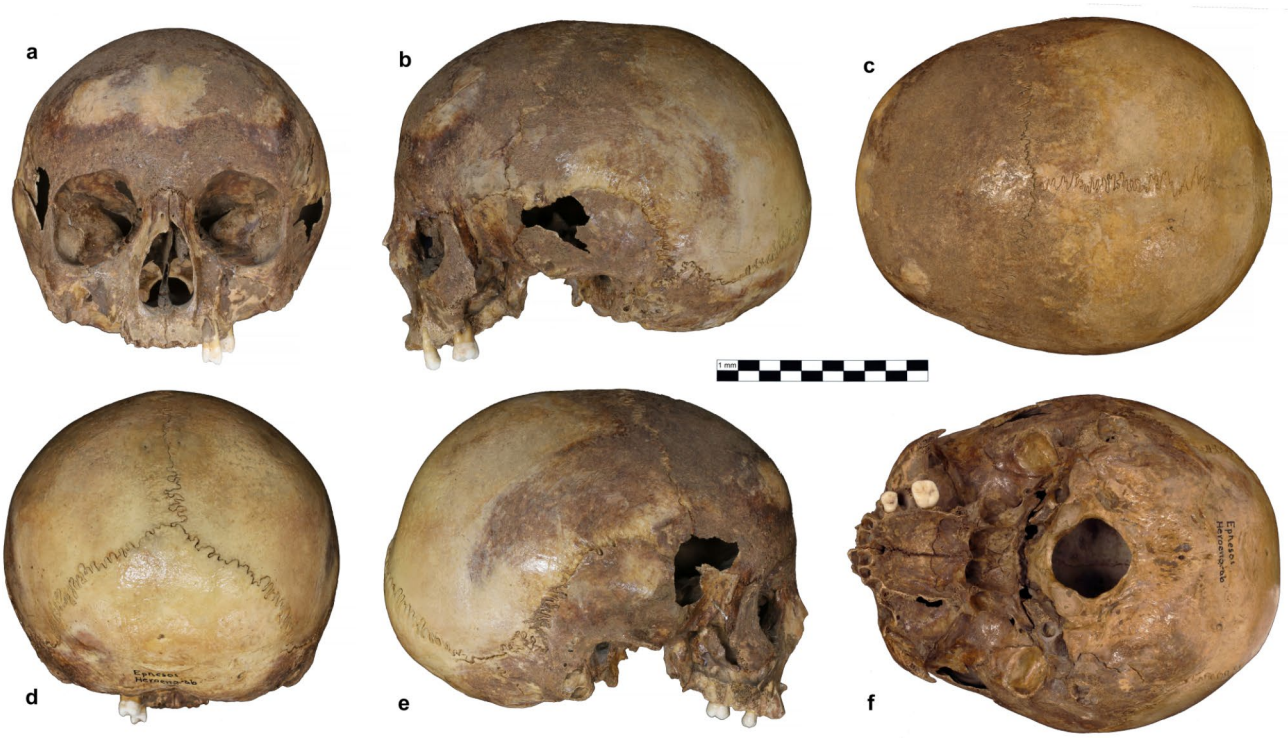

Fig. 1. The cranium from the Octagon in Ephesos. Six norm views: (**a**) frontal, (**b**) lateral sinistra, (**c**) vertical, (**d**) occipital, (**e**) lateral dextra, (**f**) basal.

Measurements	Weber et al. 2024	Weninger[11]
Max. Cranial Length (g-op)	178 mm	178 mm
Max. Cranial Width (eu-eu)	145 mm	145 mm
Basion-Bregma Height (ba-br)	110 mm	110 mm
Min. Frontal Width	98 mm	98 mm
Index Length/Width	81.5 (brachycranic)	81.5
Index Length/Height	61.8 (chamaecranic)	61.8
Index Width/Height	75.9 (hyper-tapeinocranic)	75.9
Cranial Capacity	1428.75 cm3	1405 cm3
Biauricular Width	116 mm	115 mm
Biorbital Width	95 mm	96 mm
Facial Length	80 mm	80 mm
Ganzprofilwinkel	93° (hyperorthognathic)	93°

Table 1. Traditional distance and volume measurements of the cranium from the Octagon.

The right sutura occipitomastoidea is well visible and in similar condition as the other open cranial sutures. The left occipitomastoid suture is, in contrast, completely obliterated, leaving no trace of its pathway (Figs. 1f and 2). This suture commonly fuses in senile age (65 + years[18]). This craniosynostosis could partly explain the cranial deformity during growth, leading to pronounced asymmetry. The virtual endocast also shows signs of earlier suture closing of the left lambdoid suture compared to the right one, and larger transverse and sigmoid sinus on the right than on the left side (Supplementary Information Fig. S6). The sphenobasilar synchondrosis is wide open (~ 3–4 mm, Fig. 3). The right orbit is located lower than the left one (Fig. 1a) by 1.2 mm (using an anthropological norm orientation), the nasal septum is significantly deviating to the left in its upper part, as well as the Crista Galli.

The most striking trait of this cranium is nevertheless the under-developed and abnormally inclined maxilla (Fig. 1a,b,e). Weninger[11] mentioned a "weak maxilla with reduced bony substance" (p. 165) but did not go into the details of the retracted maxillary position showing a very unusual inclination of the palate and face relative to the skull base (Fig. 1b & e, Supplementary Information Fig. S8). While basicranial flexion with 137.9° is well within the normal range of modern humans (127.7 ° -153.7 °), the inclination of the palate to the foramen

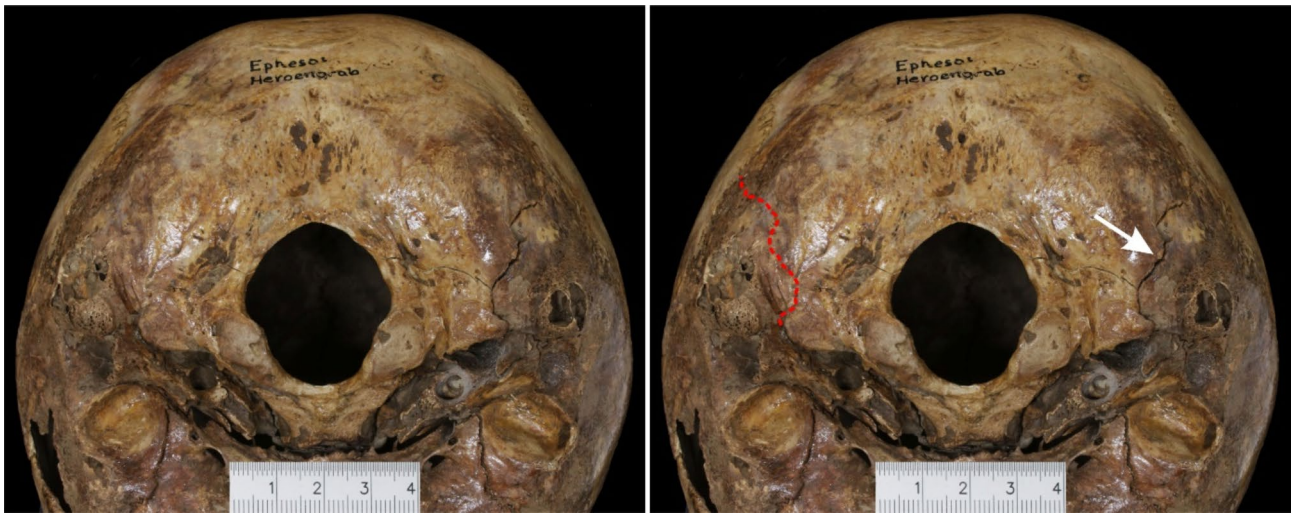

Fig. 2. The completely obliterated left occipitomastoid suture of the Octagon-cranium. On the left panel, the original status is shown. On the right panel, the position of the right occipitomastoid suture is marked with a white arrow, and the tentative pathway of the left occipitomastoid suture (red curved line) was copied from the right side and mirrored.

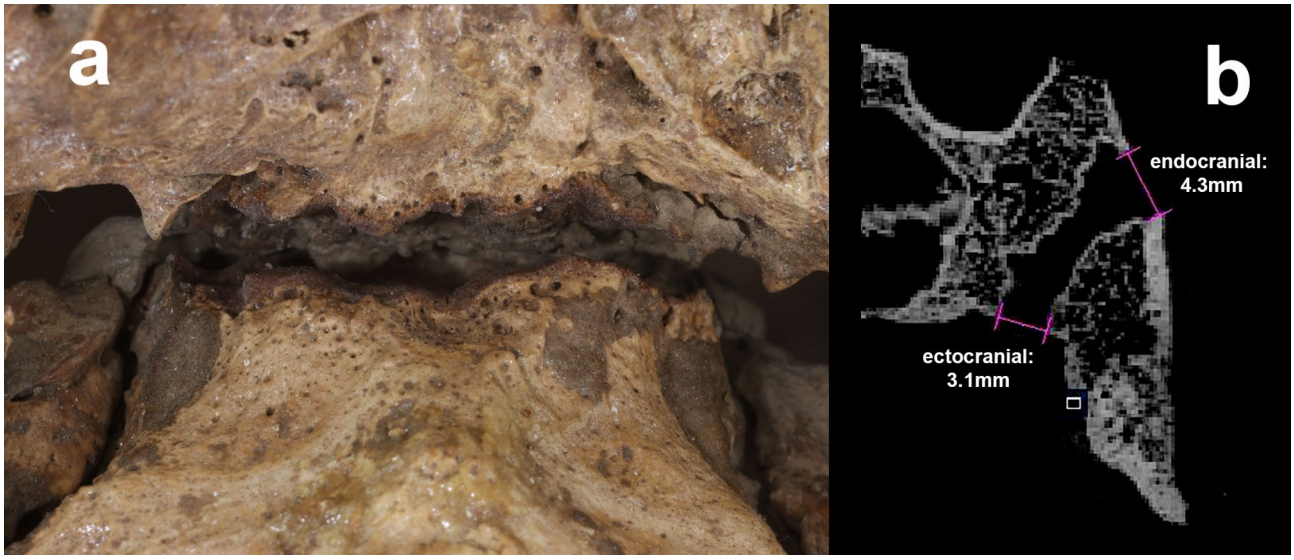

Fig. 3. The widely open sphenobasilar synchondrosis, (**a**) ectocranial surface of the original; (**b**) cut through µCT slice representing the midsagittal plane with endo and ectocranial measurements.

magnum with a value of 145.9º is outside of the variation observed in a geographically diverse sample of recent *Homo sapiens* (150.2 º -178.0 º) (Fig. 4A, Supplementary Information Tab. S3).

The abnormal position of the maxilla was not recognized in earlier studies, although it is apparent in standard visual inspections. We performed a state-of-the-art Geometric Morphometric analysis using 23 classic cranial landmarks (see Methods). Figure 4B demonstrates the exceptional morphology of the Octagon-cranium, as none of the 42 other crania, sampled from five continents, comes close to its particular shape. We also compared the Procrustes distances in shape space between the original and the respectively mirrored specimens to determine the degree of individual asymmetry. The Octagon-cranium is the most asymmetrical in our sample, with an extreme Procrustes distance of 0.065 (mean = 0.032, S.D. = 0.010), thus out of 3 S.D.s from the mean of asymmetry.

The teeth

In occlusal view, the M^1 shows an unworn surface without any shiny spots. There is thus no evidence that this tooth had any static, supporting, or dynamic contact with its antagonist (Fig. 5). This suggests that it was not in functional use although the M^1 is generally the first permanent tooth to erupt in the upper jaw. Occlusal fissures,

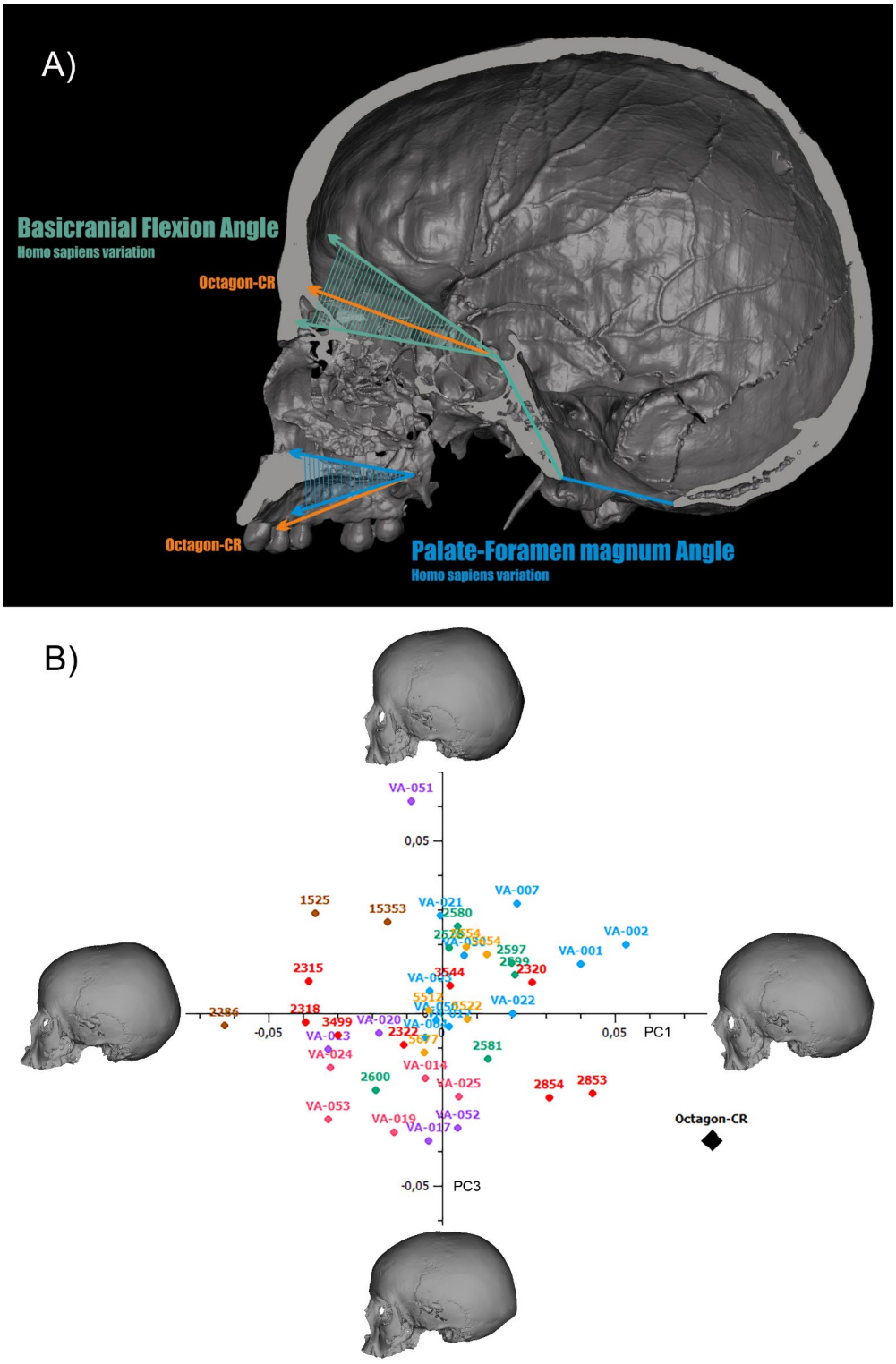

Fig. 4. Facial shape and deformations. (**A**) While basicranial flexion of the Octagon cranium (upper orange arrow) is well in the range of modern humans (turquois arrows), the inclination of the palate to the foramen magnum (lower orange arrow) exceeds the values of the comparative sample (blue arrows). The cut cranium shown is the one from our sample closest to the mean. (**B**) First and third principal components of the cranial shape analysis. 23 classic landmarks on crania were used. PC1 explains 18.1% of total variation, and PC3 11.8%. The extremes of related shapes are indicated for each axis. Red – East Africa, pink – South Africa, orange – Egypt, purple – Australia, brown – South America, green – East Asia, blue – Europe, black – Octagon Cranium (sample in Supplementary Information Table S3).

Fig. 5. Bucco-occlusal view of the upper M^1 and P^3 still in situ. While the later erupting first premolar already shows significant wear on the buccal cusp, the first molar displays absolutely no signs of use. Note also the lingually inclined position of the premolar.

particularly the distal one, are covered by a foreign material. The buccal surface exhibits dental calculus. Subtle signs of hypoplasia are suggested at the distobuccal and mesiolingual cementoenamel junction. The µCT images reveal numerous cracks in the enamel and dentin material. Some dark bands closely below the enamel-dentin junction (Supplementary Information Fig. S9b, S18a, S18b) differ from the common cracks in being broader and more diffuse. These might indicate interglobular dentin (IGD) which would suggest vitamin-D deficiency[19,20]. Initial caries is seen mesially in the former contact area with the P^4 and on the mesiobuccal root surface. The P^3 is noticeably lingually inclined and presents a black discoloration in the mesiodistal fissure. Subsequent analyses did not confirm carious demineralization. Brown dental calculus is present on the enamel and mesially between the buccal and palatal roots. In contrast to the M^1, the P^3 presents distinct signs of wear, particularly a concave deepening on the buccal cusp tip featuring dentin caries, and four cracks initiating from the worn cusp tip commencing in mesial, distal, buccal, and lingual direction. Fractures that continue along the root deep below the alveolar bone level can be found on the whole buccal part of the tooth. The unstable condition of the P3 caused bone resorption on the buccal alveolus wall. We therefore conclude that these cracks emerged ante mortem (for a more detailed description of the teeth see Supplementary Information).

Altogether, we found mild caries affection, minimal signs of developmental disturbances (hypoplasia), and no peculiarities regarding roots and nerve canals. Comparing the 3D shape and size of the tooth crowns of the P^3 and M^1 with a geographically diverse sample, there are no peculiarities to report, either in shape or in size (Supplementary Information Fig. S1, S2, S3, S4 and Tab. S1). From a functional perspective, the complete absence of wear on the M^1 compared to the observed wear and fracturing of the P^3 is remarkable. Strong wear, as well as fracturing and subsequent alveolar bone resorption, may result from functional overload and improper occlusal relations. Given the range of age estimated between 11 and 14 years (see below), the M^1 should have been in function for five to eight years, while the P^3 usually erupts four years later; thus, it should not show more significant wear and damage than the M^1. With that in mind, we doubt that the M^1 had ever been in functional occlusion with its antagonists. The absence of wear is thus rather not the result of a non-abrasive diet but of a masticatory malfunction. The vertical orientation of the maxillary arch and the angulation of the mandibular fossae suggest a vertical maxillary overgrowth and a potentially retrusive undersized mandible.

Age at death

The root growth of the P^3 was completed. Still, the apex mineralisation was not yet terminated (Supplementary Information Fig. S9a). According to published standards from modern populations this would correspond to a male mean (see genetic results) of 11.4 years ± 1.0 years S.D. and a median of < 13 years in a sizable Japanese sample of orthopantomographs ("*Rc*" in[21]), or a male median of 12–13 years (range 10–14 years) in a large Turkish sample of panoramic radiographs ("*G*" in[22]).

The roots of the M^1 were completed and apex mineralisation already terminated {male median 9 years ("*Ac*" in[21]); male median 11 years, range 10–12 years ("*H2*" in[22])} (Supplementary Information Fig. 9b). The partially preserved alveoli of both maxillary M^2s show that the teeth already erupted, with the distal root developed at least to three quarters {(Fig. 6; male mean 12.1 years ± 1.1 years S.D., median 12 years ("*R3/4*" in[21]; male median 12 years, range 10–13 years ("*F*" in[22]}. Weninger[11] confirms this state, describing the roots of the two upper M^2s as not yet closed, which cannot be verified due to the absence of the teeth. The lingual wall of the crypt of the left M^3 is well visible and shows that the M^3 was not yet erupted (Fig. 6; alveolar emergence in males > 18 years in[23]). The mean age for an open sphenobasilar synchondrosis in males has been determined to be 12.3 years ± 2.7 years S.D. in a large Iranian sample of cadavers and was established as a reliable indicator for age estimation[24].

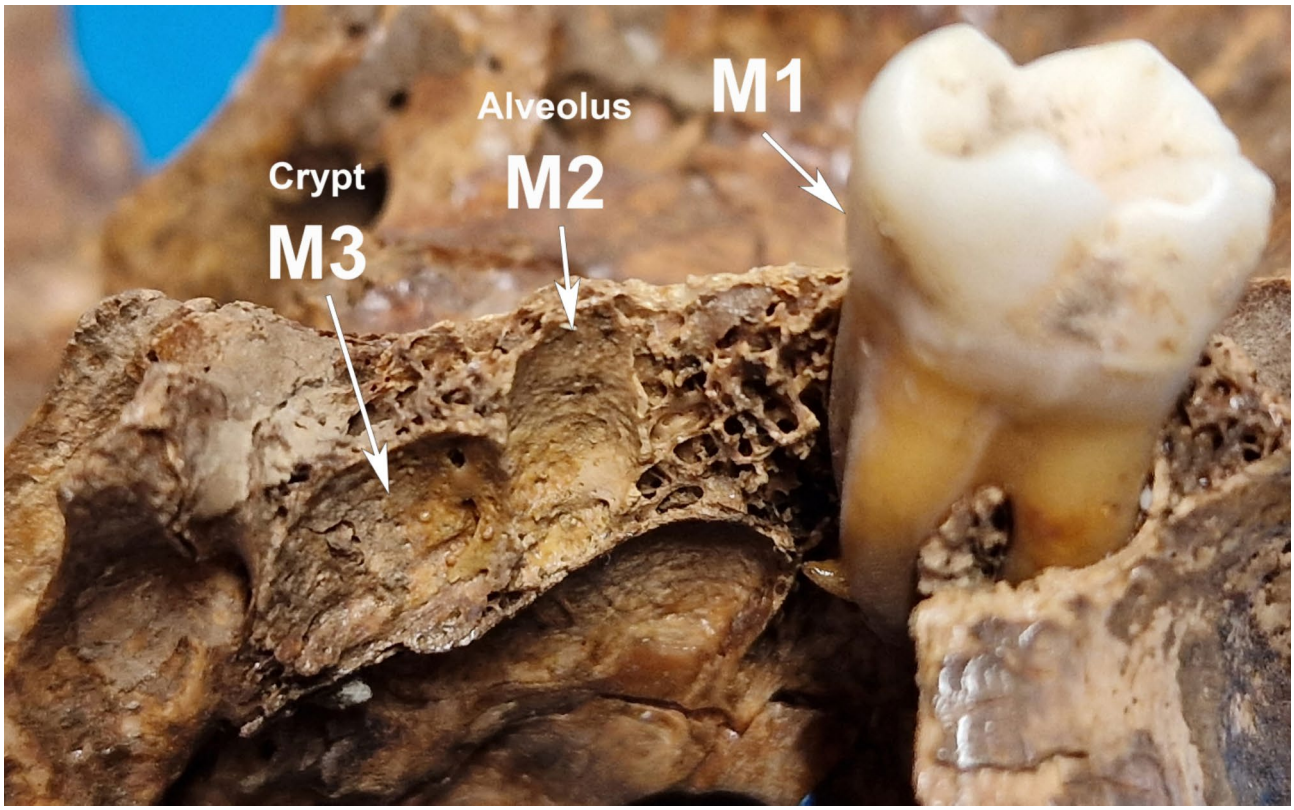

Fig. 6. The partially preserved alveolus of the upper second molar (M^2) and crypt of the upper third molar (M^3) in the left maxilla. The upper first molar (M^1) is still in situ.

The Octagon-cranium showed a completely open synchondrosis on the ecto- (3.1 mm), as well as endocranial (4.3 mm) surface (Fig. 3). This supports the dental age perfectly since a complete fusion is reported between 15 and 19 years in males[25,26], starting with the endocranial fusion first. Moreover, open synchondrosis has never been observed in males after 13 years of age[27]. Due to the large variability of this trait, influenced by nutrition, health status, and growth rate, some authors see it as limited for age determination[28].

Altogether, the dental status and the developmental stage of the sphenobasilar synchondrosis of the Octagon-cranium suggest an age of the individual in a plausible range between 11 and 14 years. Our cranial estimate results in a younger age than the 15 to 17 years derived from the post-cranium[12] and by the first descriptor of the cranium (16–17 years in[11]). However, we cannot exclude the possibility of developmental differences, which could have occurred during the past two millennia, or differences between various geographical populations. Still, we find it highly unlikely that the Octagon individual was already in their late adolescence rather than early puberty.

Dating the cranium

To radiocarbon date the cranium, we took bone powder from the petrosal bone (see Methods). Sample pretreatment for bones followed collagen extraction and ultrafiltration protocols outlined in[29,30]. We obtained 6.5 mg of collagen from 260 mg of bone (2.5% yield) following ultrafiltration. Sample ^{14}C activity was measured with the graphitization, target preparation and AMS measurement undertaken after[31,32].

Calibrating the result using the INTCAL20 (terrestrial) curve[33] we obtain a calibrated age range of 355—282 (58.4% prob.) and 231—170 cal BC (37.0% prob.) at 95.4% probability (Fig. S10). The multimodal distribution is a function of the wiggles in the calibration curve through this period.

Bone collagen $\delta^{13}C$ and $\delta^{15}N$ values were also measured independently using an EA-IRMS (Elemental Analyser/Isotope Ratio Mass Spectrometer) to a precision of ± 0.3 per mil relative to VPDB (Table S2). We observe that the values ($\delta^{13}C$ and $\delta^{15}N$ values were -19.1 and 11.3‰ respectively) indicate the possibility of a reservoir effect of the kind caused by the dietary uptake of foods from different radiocarbon reservoirs. Estimating the precise amount of offsets from the true age is difficult in the absence of isotopic evidence from other humans or animals in the local site. To correct the radiocarbon estimates we used an endpoint correction approach. We estimated the $\delta^{13}C$ terrestrial carbon endpoint value at -21‰ and -12‰ for marine carbon, and estimated a ~ 21% possible marine food contribution, based on the measured $\delta^{13}C$ value we obtained for this sample. To re-calibrate the radiocarbon result, we used a "Mixed_Curves" approach in OxCal to quantify this, along with a ΔR value of -142 ± 66 year[33,34]. We included an uncertainty of ± 10% on the marine food estimate in the Bayesian model due to the absence of comparative data from the site location and the possibility of variation in the exact protein component of this individual. We obtained a calibrated range between 205-36BC

(89.7%), 345-317BC (4.8%) and 12-1BC (1%) at 95.4% probability (Fig. S11), which we conclude is the best estimate for the age of the cranium. This age is in good agreement with earlier dating results obtained from the femur midshaft by the A.E. Lalonde AMS Laboratory (Ottawa/Canada, see Methods) which gave a calibrated age range between 48BC-54AD (95.4%). A further study from Kanz and colleagues[12], also using the femur midshaft, reports a radiocarbon date range between 210 and 20 BC (94% prob.) obtained at the Vienna Environmental Research Accelerator (sample VERA-4104), which is also in good agreement with our corrected results above.

Genetic results from the cranium and post-cranium

Genetic analysis was used to evaluate important questions such as the sex, genomic ancestry, and whether the three different skeletal elements (cranium, femur, rib) belonged to the same individual. Each element was individually sampled and processed as described in the Methods section. The recovered DNA's quality and authenticity was assessed first by calculating the endogenous contents for each skeletal element after removal of duplicated reads, accounting for 0.02% for the rib, 0.08% for the femur, and 38.42% for the cranium, leading to average genomic coverages of 0.0002X, 0.0020X, and 1.6656X, respectively (Supplementary Information Tab. S4). Deamination patterns typical of ancient DNA supported the authenticity of the recovered DNA of all three elements, with terminal deamination frequencies on the 5' end of DNA sequences of 13% (rib), 19% (femur), and 25% (cranium) (Supplementary Information Fig. S12, Supplementary Information Tab. S4). Similarly, contamination estimates on mitochondrial[35] and X-chromosome reads[36] yielded a maximum of 1.71% (95% CI 1.54–1.89) for the cranium, well below the typically accepted threshold of 5% in ancient DNA studies (Supplementary Information Tab. S4).

Genetic sex estimation quickly clarified that the skeleton cannot be attributed to Arsinoë IV since the cranium and the femur belong to male individuals, while the low amounts of data for the rib are suggestive of a male as well, although with some uncertainty (Fig. 7C, Supplementary Information Tab. S4). However, due to the limited amounts of data available for the femur and rib, only the cranium and femur pair had enough overlapping data meeting the minimum requirements of the relatedness estimators TKGWV2[37] and READv2[38] for the identification of "Identical/Twins". The results from both methods agreed on that classification (Fig. 7D, Supplementary Information Tab. S5). Despite the much lower amount of overlapping data, a similar relationship is suggested for the cranium-rib pair, but the statistical power to support such claim is non-existent. However, the estimated mitochondrial haplogroup of the rib sample (H5'36) is ancestral to the cranium and femur's H5d, with 7 out of 9 polymorphisms shared between the rib and the cranium, providing further support for the individuals to, at least, be potentially closely related (Supplementary Information Tab. S4). In ancient populations, these haplogroups have so far been found in Bronze Age Germany[39], in an individual from Bronze Age Israel (I2198 in[40]), another from Etruscan Italy (VET001 in[41]), and lastly a Punic individual from Sardinia (MS10577 in[42]).

We performed population genomic analyses on the cranium data to understand the possible geographic origins of the Octagon individual's ancestry. A principal component analysis (PCA) of a dataset that included modern and ancient West Eurasians placed the Octagon individual very close to ancient Bronze and Iron Age genomic variation from Southern Europe, effectively overlapping individuals from the Italian Peninsula recovered from Etruscan and Roman Imperial contexts[41,43,44] (Fig. 7A). Using a recently developed method that allows the determination of genetic similarity probability maps over time and space using PCA and chronological data[45], we found that the highest similarity probability for this individual's ancestry can be found in between the central region of the Italian Peninsula and the island of Sardinia, around 500 BC, matching the location of the PCA's Etruscan and Early Roman Republic individuals (Fig. 7B). Looking at points in time closer to his death, based on the ^{14}C interval of $205-36$ BC, we find slightly lower similarity probabilities in that region, but with the point of highest similarity almost geographically unchanged (Fig. 7B).

To understand if there were statistically significant differences between the affinities of the Octagon individual and populations from the Italian Peninsula and Sardinia, we ran f4-statistic tests of the form f_4 (Mbuti.DG, Octagon-cranium; Sardinia_BA_Nuragic, Italy_IA_Republic.SG/Italy_Etruscan). The results suggested that the Octagon cranium was significantly closer to Nuragic Sardinians than to the Etruscan groups ($-5.095 < Z < -2.730$), whereas for Italy_IA_Republic.SG the result was not statistically significant for $|Z| > 3$, although it was still suggestive of more allele sharing with Sardinians ($Z = -2.329$) (Supplementary Information Tab. S6). These results support the genetic similarity probability maps and explain the intermediate position of the highest point of similarity between mainland Italy and Sardinia. We further checked if other Italian, Spanish, and diverse Balkan groups were closer to the Octagon individual than the Nuragic Sardinians, but the results were unchanged. The same was true for two other tests using Hellenistic and Roman period individuals from Western Turkey ($-7.193 < Z < -6.116$) (Supplementary Information Tab. S6).

Lastly, we also investigated the presence of runs of homozygosity (ROH) in the cranium sample using hapROH[47], as a proxy for population inbreeding, but found no segments longer than 4 centimorgans and therefore no support for such reproductive practice (Supplementary Information Fig. S16).

Discussion

Based on genetic data, the cranium from the Octagon is a male, and thus is not representing Arsinoë IV. There are no signs of any sex chromosome disorders such as Klinefelter syndrome or others. All genetic data, including the uniparental haplogroups, support an origin of his recent ancestry in the Italian Peninsula or Sardinia. These facts are well compatible with an individual living in Ephesos during the Classical Roman period, two thousand years ago. Further genetic results from the femur from the Octagon postcranial findings (rib fragment data proved to be insufficient) suggest that it belonged to the same individual as the cranium. The radiometric ^{14}C-dating, considering dietary offsets, fits the reported lifetime period of Arsinoë IV. It remains unclear when and how the postcranium was removed from the sarcophagus and scattered in various other places of the Octagon, which could have happened during Keil's excavation 1929 or any time after until 1982. Keil[3] just confirmed that they

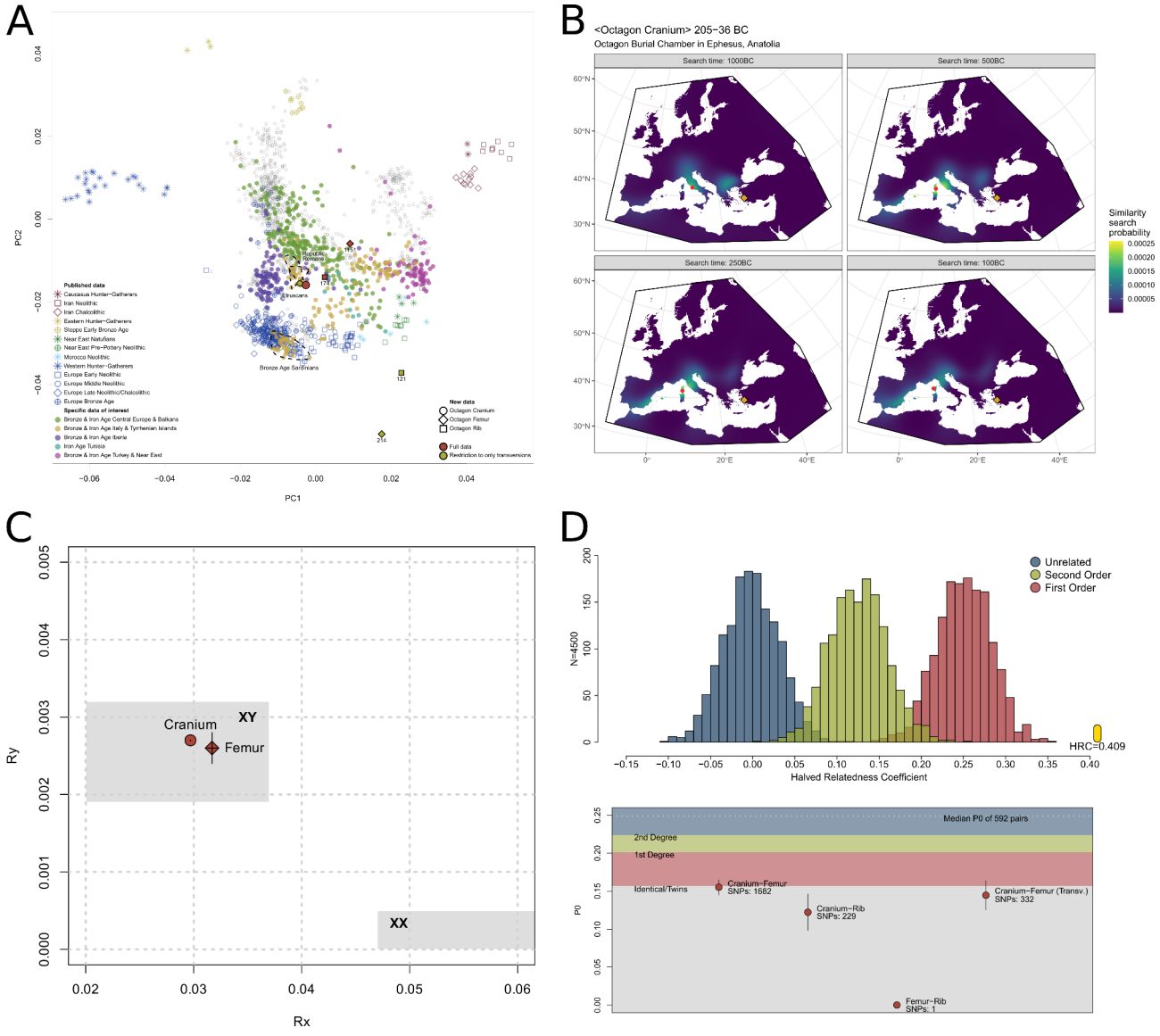

Fig. 7. Summary of the genetic results. (**A**) PCA of modern West Eurasian populations with ancient data projected onto the two first PCs. Numbers under symbols represent the sample's corresponding SNP (Single-Nucleotide Polymorphism) numbers in this analysis. (**B**) Genetic similarity probability maps for the period of death of the Octagon individual, based on ^{14}C dates, and for three other preceding periods, where higher similarity probabilities are found[45]. (**C**) Genetic sexing results for the cranium and femur based on ratios of sequences aligning to the X and Y chromosomes[46]. Grey areas represent expected XY and XX distribution ranges, and crossed lines the standard error. (**D**) Relatedness estimation results using TKGWV2 (Top) and READv2 (Bottom). The top panel shows the simulated population coefficients after 1500 simulated relationships, based on 1644 overlapping SNPs between the cranium and the femur, that produced a Halved Relatedness Coefficient (HRC) of 0.409, above the simulated distribution for 1st degrees, and therefore suggesting an "Identical/Twins" relationship. The bottom panel shows the pairwise results for the three elements, as well as the result for the cranium-femur pair when restricting the genetic data to only transversions.

carefully closed the grave chamber (p. 44), but did not mention what happened to the postcranium. Similarly, the fates of the mandible and the missing teeth remain open.

The morphological investigations of the cranium contradict earlier research and show strong signs of asymmetry, deformations, and malfunctions. Most strikingly, the maxilla is underdeveloped and abnormally vertically inclined. The whole cranium shows a basal flexure, the left occipitomastoid suture is completely obliterated while the right one is still completely open, the occipital condyles show severe defects, and the mandibular fossae show an extreme angulation in relation to the midsagittal plane of the cranium. The Octagon-cranium falls entirely outside the cranial morphological variation of a geographically diverse sample, is the most asymmetric in this sample, and shows the lowest Palate to Foramen magnum angle. The upper first molar

does not indicate any sign of use, suggesting that it had never been in functional occlusion with its antagonists, while the later erupting upper first premolar shows an unusual lingual orientation, and wear and ante-mortem fractures on the buccal cusp which may result from functional overload and improper occlusal relations. The vertical orientation of the maxillary arch, the strong angulation of the mandibular fossae, and the wear state of the teeth suggest an underdeveloped mandible, a retrusive mandibular relationship, and masticatory malfunctions. Based on the developmental stage of the teeth and the sphenobasilar synchondrosis, the tentative age at death of the individual can be defined in a range between 11 and 14 years.

Pronounced asymmetry and hypoplasia generally reflect genetic and environmental pressures experienced throughout development. Developmental stress and instability provisionally contradict earlier findings on the postcranium and cranium. Weninger[11] saw the Octagon individual as a person representing *"… a refined, specialized type of the ancient world of high culture …"* and *"…a very distinguished personality…"* (p. 168). Our data cannot be used to draw inferences about social status, but we showed that the development of this cranium was accompanied by severe problems and disturbances which are compatible with any social strata. Our cranial results are in mismatch with those from the postcranial analysis, where no signs of illnesses and stress markers were detected[12].

The cause for developmental disturbances can be manifold. Premature craniosynostosis, for instance, could possibly be related to conditions such as thyroid dysfunction[48], rickets, and other metabolic disorders[49]. Due to the taphonomic processes acting on the upper first molar and the insufficient µCT scan resolution we cannot confirm with certainty the diagnosis of interglobular dentin (IGD) which could indicate a vitamin-D deficiency during tooth formation[19,20]. If this was the case, it should have happened shortly before or after birth because the potential IGDs are found 0.2–0.4 mm below the enamel-dentin junction. A dentinal growth rate of 3–5 µm per day is suggested for permanent tooth formation[50], and first permanent molars start to develop around the 30st week after fertilization[51]. Another genetic disorder, the Treacher Collins Syndrome (TCS), shows several phenotypic overlaps with the conditions of the Octagon-boy. TCS is autosomal dominant and affects both males and females. It is frequently associated with a rotation of the occlusal plane, mandibular micrognathia, open-bite malocclusion, down-slanting eyes, brachycephaly, dental anomalies, and conductive hearing loss[52]. Patients with TCS also show an extreme inclination of the palate to the skull base and an unusual flexion of the cervical spine. Despite the reasons for such a craniofacial configuration, for a normal view, the head must be extremely raised in relation to the spine. Avoiding this hyperextension of the cervical vertebrae, on the other hand, would restrict the gaze to the ground. This could explain the defects on the occipital condyles of the Octagon-boy, despite his young age (Supplementary Information Fig. S7). The particular craniofacial morphology is further associated with functional, as well as with aesthetic and subsequent psychosocial problems. The appearance of the Octagon-boy can probably be conceived similar to a TCS patient. However, the coverage of our genetic sampling was not sufficient enough to prove genetic disorders such as TCS or others.

The construction date of the Ephesos Octagon is still discussed, but there are reasonable assumptions that there was a time gap between Arsinoë IV's murder and the completion of the building of at least several decades[4–6]. This considerable gap was always a cause for debate as to whether the Octagon was the last resting place of Arsinoë IV. What we can now say with certainty is that the person buried in the Octagon was not Arsinoë IV, and the search for her remains should continue. In addition, a wide range of new research questions are open regarding the origin, fate and social background of the Octagon-boy. Despite a lack of local Anatolian contemporaneous genetic data, he was possibly a member of the Romans living in Ephesos, and future analyses of strontium isotopes might help understanding whether he was born and raised locally or arrived from abroad.

The hypothesis that the Octagon was built in honour of Arsinoë IV is no longer a parsimonious one. Nevertheless, based on its architectural analysis and archaeological interpretation[2,4,13], the tomb could still be connected to a person of significant social status somehow linked to the Egyptian cultural sphere. Arsinoë IV is one such person who would fit this presumed background, but other people, probably currently even unknown to history, can and should not be disregarded. As our analyses show, should there have been an attempt to disinter and relocate the human remains of Arsinoë IV into this tomb after its construction was finished, it apparently was not successful. Why this 11-14-year-old boy suffering from significant developmental disturbances was buried in such a prominent building within the Ephesos urban area also remains unexplained for the moment. Even experts 2,000 years later were persuaded that these bones would represent a young, healthy female[11,12]. We hope that with our work, the view on Arsinoë IV became less clouded by anecdotes and speculations, and her and the Octagon-boy's fate can be unravelled free of bias in the future.

Methods

Micro-CT scanning of the cranium

The Octagon-cranium was scanned on the 21st of December 2022 at the Vienna Micro-CT Lab at the University of Vienna with a VISCOM X8060 Scanner (71 µm, 130 kV, 330µA, 1400ms). A second scan was performed on the 3rd of January 2023 for the maxilla and teeth (22 µm, 130 kV, 280µA, 1700ms). The scans were taken before the genetic and dating sampling to archive the anatomy, and 0.75 mm copper filters were used to protect the DNA as best as possible.

Geometric morphometric analysis of the cranium

A diverse sample of 42 crania from various geographical populations (East Africa, South Africa, East Asia, Egypt, Australia, South America, Europe) from the Department of Evolutionary Anthropology, University of Vienna and the Natural History Museum Vienna was used to include a maximum of morphological variation for the comparison of cranial shape and angles (Supplementary Information Tab. S3). Tomographic data was obtained from medical CTs and µCTs. After segmentation of the bony structures, 3D surfaces were extracted and landmarked in Amira 3D (www.thermofisher.com). The set of 23 landmarks comprises Prosthion, Nasospinale,

Rhinion, Nasion, Glabella, Bregma, Lambda, Opisthocranion, Inion, Opisthion, Basion, Porion left & right, Maxillofrontale left & right, Orbitale left & right, Frontomalare orbitale left & right, Torus inferior left & right (upper edge of orbit at foramen/sulcus or lateral rim of depression), and Alveolus upper M1 left and right (mid of upper M1 alveolus). For Geometric Morphometric (GM) analysis we used the EVAN Toolbox 1.75 (www.evan-society.org). A virtual endocast of the Octagon-cranium was also produced in Amira 3D. All Virtual Anthropology procedures are described in[53]. For the estimation of the basicranial flexion, we measured the flexion between the Basion, Sella turcica (midpoint-area), and Foramen caecum[54] (Supplementary Information Fig. S15). To determine the inclination of the Palate to the Foramen magnum, four landmarks were digitised on the flat Lamina horizontalis of the palate and four landmarks on the Foramen magnum (Supplementary Information Fig. S14). Each set of four landmarks defined a best fit plane and the angle between these planes in the mid-sagittal projection was measured.

Dating of the cranium

A sample of 260 mg was taken from the Octagon-cranium from the right carotid canal on the 28th of September 2023 by one of the authors (TH) and was further chemically pretreated and prepared at the Higham Lab, Department of Evolutionary Anthropology, University of Vienna. Sample pretreatment for bones follows collagen extraction and ultrafiltration protocols outlined in[29,30]. The sample was measured at the Keck AMS facility, University of California at Irvine. For details on aspects of target preparation and AMS measurement see[31,32]. Radiocarbon dates are reported in radiocarbon years BP (Before Present - AD 1950) using the half-life of 5568 years. Isotopic fractionation has been corrected for using the $\delta^{13}C$ values measured on the AMS. $\delta^{13}C$ and $\delta^{15}N$ values are also measured independently using an EA-IRMS (Elemental Analyser/Isotope Ratio Mass Spectrometer) to a precision of ± 0.3 per mil relative to VPDB. These are reported in Supplementary Information Tab. S2 .

An earlier dating was performed at A.E. Lalonde AMS Laboratory, Ottawa/Canada in 2017 using the powder obtained from the femur midshaft (see Genetics Sampling below). Radiocarbon analyses were performed on a High Voltage Engineering (HVE) 3MV tandem accelerator mass spectrometer. For the calibration OxCal v4.2.4[55] and the IntCal13 calibration curve[56] were used. Sample pretreating techniques and definitions of material codes are described in[57].

Genetics

Sampling

The genetic sample from the Octagon-cranium was taken at the Pinhasi Lab at the Department of Evolutionary Anthropology, University of Vienna by one of the authors (OC) on the 10th of January 2023 from the right cochlea. The femur and rib fragments used in this study originate both from the right side of the individual. Samples were made available by the Austrian Archaeological Institute. The postcranial skeleton is kept in the depot of the Austrian excavation house at Ephesos. The femur samples were taken from the midshaft by Gro Bjørnstad cutting a slice of the femur with a hacksaw using protective gloves and cleaning the equipment with ethanol beforehand. The samples were exported with the friendly permission of the General Directorate for Cultural Heritage and Museums in Ankara.

The samples were processed in dedicated ancient DNA facilities at the Department of Evolutionary Anthropology of the University of Vienna. The cranium's cochlea was sampled using a protocol that allows access to it from the cranial base with minimal damage[58]. For the femur, the same powder obtained for the ^{14}C dating analyses was used (see above). A fragment of the rib was sampled by first cleaning any surface contamination using a dental sandblaster, and using the same method to isolate a small fragment that was subsequently milled to homogeneous powder in a Retsch ball mixer mill MM 400 at maximum frequency (30 Hz) for 1 min, with a 10-sec pause after the first 30 s, to avoid heat built up that could damage the ancient DNA.

DNA extraction, library preparation, and DNA sequencing

The DNA from each sample powder was extracted using the protocol developed by Dabney and colleagues[59], but using preassembled high pure viral nucleic acid large-volume kit spin columns from Roche[60] instead of the protocol's original MinElute column apparatus. Double-stranded DNA libraries were prepared according to a modified Meyer and Kircher[61] protocol. Individual libraries were prepared from 12.5 µL extract each, and intermediate clean-up steps were performed using Qiagen MinElute PCR purification kits to retain very short fragments (~30–80 bp). Before amplification, real-time qPCR of a small quantity of library (1 µL) was performed to assess the number of molecules present and choose the required number of cycles for amplification. All libraries were then double-indexed and amplified using NEBNext Q5U Master Mix DNA polymerase. Before sequencing, libraries were quantified using Qubit and TapeStation. The libraries were then screened on an Illumina NovaSeq SP SR100 XP, and deeper sequenced on an Illumina NovaSeq X SR100 10B XP at the Vienna BioCenter Core Facilities.

Once the three available skeletal elements – cranium, femur, and rib – passed the initial screening for ancient DNA quality and authenticity, they were sent for deeper genomic sequencing. A focus was put on producing enough data for the cranium and femur to have minimum amounts of overlapping data to evaluate their biological relationship. The rib produced much smaller quantities of data, despite it looking authentic based on metrics such as DNA fragment lengths and deamination patterns. The library was therefore enriched using a custom-designed set of baits to allow enough sequencing for further analyses (Supplementary Information Table S7).

Data processing and authentication

Library adapters and barcodes were removed from the raw sequencing data with cutadapt (v3.5)[62], allowing for 1-bp overlap and excluding sequences shorter than 25 base pairs (bp). The sequences passing this filter were aligned to the human reference genome hg19, with the mitochondrial genome replaced by the Revised Cambridge Reference Sequence (RCRS), using the "aln" command from the Burrows-Wheeler Aligner (BWA) (v0.7.17-r1188)[63], with seeding disabled by using the argument "-l 1000". Sequence alignments were then converted to the SAM format using BWA's "samse", and then converted to BAM format with SAMtools "view" (v1.3.1)[64] discarding unmapped sequenced by using the argument "-F 4" and restricting to a minimum quality threshold by using "-q 30". Next, we used SAMtools' "rmdup" command to exclude duplicated sequences with exact coordinates and length.

Sequence deamination damage was assessed with mapDamage (v2.0)[65]. Contamination was assessed on the haploid X chromosome of males using hapCon with a threshold of 0.02× or 2000 SNPs[66], as well as on the mitochondrial genome using schmutzi[35]. Genetic sex and chromosomal aneuploidies for the cranium and femur were determined by looking at the ratio of sequences aligning to the X and Y chromosomes compared to the total fraction aligning the autosomes[46]. As the data from the rib was produced with a custom-designed set of baits, sex estimation was based on the expected number of reads for XX and XY individuals. Considering the number of SNPs for chromosome X (6635) and chromosome 7 (8681), which have similar physical lengths, in the baits set, an individual with two copies of chromosome X would in theory produce ~ 24% less chromosome X reads than those for chromosome 7. In the case of the rib, we obtained 467 reads for chromosome 7, but 46% less for chromosome X, with 253 reads, suggesting that the individual might have had only a single copy of the latter chromosome. Chromosome Y had 15 reads aligned to it. However, due to the low amounts of data, capture bias or contamination could very easily impact these ratios, so we view this result as tentative but not definitive.

Before further analyses, 6 bp were trimmed from the ends of every sequence in order to remove deaminated bases that could introduce unwanted bias. For this we used the "trimBam" function from the package BamUtil[67]. To estimate Y haplogroups we used Yleaf[36] on the alignment files after duplicated reads removal, and for mitochondrial haplogroups we re-aligned the raw sequencing data to the mitochondrial RCRS using the same parameters described above, and then used SAMtools "consensus" from version 1.19.2 to create a consensus sequence that was uploaded to HaploGrep3[68].

Principal component analysis

The 6-bp trimmed files were used to extract pseudo-haploid genotypes for 1,233,013 positions on the human genome ("1240K capture set") by randomly selecting an allele at each position and duplicating it. We used a subset of 1,004,658 modern[69,47] and 23,321,898 ancient West Eurasians[39–41,43,65,70–96] for principal component analysis using the "smartpca" tool from the software package EIGENSOFT[97]. The options shrinkmode and lsqproject were both set to "YES", with the latter projecting all ancient individuals onto the eigenvectors computed on the modern populations. We included a version of each of the 3 samples using transverion SNPs only to evaluate potential biases caused by deamination within the reads. The output from "smartpca" was then used as input for Mobest, in order to spatiotemporally map the genetic profile of the Octagon individual[45]. Geographical coordinates and median sample dates for the ancient individual matrix were retrieved from the Allen Ancient DNA Resource (AADR)[98]. The template script provided by the authors was used to run the pipeline, with the final run using a spatial cell size of 10 km, and four times selected in order to investigate the past distribution and potential most likely origin of the individual's ancestry: 1000 BC, 500 BC, 250 BC, and 100 BC.

Relatedness estimation

To investigate if the three samples belonged to the same individual we used two relatedness estimation methods. First, the Thomas Kent Genome Wide Variants version 2 (TKGWV2) method was developed specifically for ultra-low coverage ancient DNA data, harnessing the power of using population allele frequencies to increase its accuracy with very little data[37], and so it appropriately suited this project. The second method used was Relatedness Estimation from Ancient DNA version 2 (READv2), which is an updated version of the most popular relatedness estimator for ancient DNA, uses pairwise mismatch rates on different windows along the genome to produce relatedness estimates[38]. For TKGWV2, we estimated relatedness both using genome wide data and the 1240 K capture set. For the former, we used the allele frequency data available from TKGWV2's publicly shared data, which contains ~ 22 million bi-allelic SNPs from modern European individuals, as previous research suggested that they introduce little bias even on past populations back to Neolithic times[37]. However, we also used the 1240 K SNP set with allele frequencies from populations genetically close to the Octagon individual, (the exact individual labels are presented in Supplementary Information Table S5) based on the results of the population genomic analyses, in order to confirm the earlier results. For READv2, we used a set of 22 individuals from Bronze Age Sardinia (individual labels in Supplementary Information Table 5) as the base population to obtain a median relatedness value. To get further confirmation of these results, we also restricted the READv2 analysis to 260,390 transversion SNPs within the 1240 K dataset and reanalysed the cranium-femur pair.

f-statistics

To investigate whether the Octagon individual was genetically closer to one population or another, we used f_4-statistics tests, within the software package ADMIXTOOLS[69]. For the outgroup population we selected Mbuti.DG, and computed statistics of the form f_4(Mbuti.DG, X; Y, Z), with X as the test individual and Y/Z pairs of populations/individuals to tests against. The options "f4mode" and "printsd" were used.

Runs of homozygosity

We used hapROH on the genomic data from the cranium (the only sample with more than the minimum threshold of 400,000 SNPs on the 1240 K set) to investigate runs of homozygosity larger than 4 centimorgans[47] and get an insight into possible recent inbreeding.

Data availability

3D surface data of the cranium and the teeth are available in our Free Data section of the digital@rchive of Fossil Hominoids (https://www.virtual-anthropology.com/3d-data/free-data/). The raw sequencing data gener ated in this study have been submitted to the European Nucleotide Archive (ENA) with the accession number PRJEB83414.

Received: 7 July 2024; Accepted: 18 December 2024
Published online: 10 January 2025

References

1. Wiplinger, G. & Wlach, G. *Ephesos. 100 Jahre österreichische Forschungen* (Böhlau, 1996).
2. Thür, H. Arsinoe IV., eine Schwester Kleopatras VII., Grabinhaberin Des Oktogons Von Ephesos? Ein Vorschlag. *Jahreshefte Des. Österreichischen Archäologischen Institutes*. **60**, 43–56 (1990).
3. Keil, J. Vorläufiger Bericht über die Ausgrabungen in Ephesos XV. *Jahreshefte des Österreichischen Archäologischen Institutes* 26, Beiblatt 5–66 (1930).
4. Rudolf, E. & Scherrer, P. *The Octagon of Arsinoe IV in Ephesos* (Nünnerich-Asmus Verlag & Media, 2024).
5. Plattner, G. A. Zur Bauornamentik des Oktogons von Ephesos, in: Ladstätter, S. (ed.), Neue Forschungen zur Kuretenstraße von Ephesos. Akten des Symposiums für Hilke Thür vom 13. Dezember 2006 an der Österreichischen Akademie der Wissenschaften, Archäologische Forschungen 15 (Verlag der ÖAW, 101–110. (2009).
6. Waldner, A. Die chronologie der kuretenstraße: Archäologische evidenzen zur baugeschichte des unteren embolos von ephesos von der lysimachischen neugründung bis in die byzantinische zeit. *Forschungen Ephesos*. **11** (4), 89–106 (2020). Verlag der ÖAW.
7. Hölbl, G. Geschichte Des Ptolemäerreiches. *(Wissenschaftliche Buchgesellschaft*, 195–205. (1994).
8. Dio Cassius & Roman History, Volume, I. V. Books 41–45. Translated by Earnest Cary, Herbert B. Foster. (Loeb Classical Library 66. Cambridge, MA: Harvard University Press, (1916).
9. Flavius & Josephus Antiquities of the Jews XV 89; Cassius Dio, Roman History XLIII 19; (Appianos, Roman History V 9).
10. White, H. Appian. The Civil Wars. London. MACMILLAN AND CO., LTD. 1899. (1899).
11. Weninger, J. in *Beiträge zur älteren Europäischen Kulturgeschichte. Festschrift für Rudolf Egger II* (ed. G. Moro) 158–168 (1953).
12. Kanz, F., Grossschmidt, K. & Kiesslich, J. *Arsinoe IV of Egypt, sister of Cleopatra identified? Osseous and molecular challenges*. (2009).
13. Thuswaldner, B. *Das Oktogon Von Ephesos. Rekonstruktion, Deutung Und Präsentation* (Technische Universität, 2015).
14. Cashmore, L., Uomini, N. & Chapelain, A. The evolution of handedness in humans and great apes: a review and current issues. *J. Anthropol. Sci.* **86**, 7–35 (2008).
15. Chou, S. T. et al. Correlation between facial asymmetry of skeletal class III jaw relationship and morphology of the temporomandibular joint: A cone beam computed tomography study. *J. Dent. Sci.* **18**, 1031–1041. https://doi.org/10.1016/j.jds.2022.11.031 (2023).
16. Roque-Torres, G. D. et al. Correlation between midline deviation and condylar position in patients with class II malocclusion: A cone-beam computed tomography evaluation. *Am. J. Orthod. Dentofac. Orthop.* **154**, 99–107. https://doi.org/10.1016/j.ajodo.2017.10.029 (2018).
17. Sülün, T. et al. Axial condyle morphology and horizontal condylar angle in patients with internal derangement compared to asymptomatic volunteers. *Cranio* **19**, 237–245. https://doi.org/10.1080/08869634.2001.11746174 (2001).
18. Knußmann, R., Schwidetzky, I., Jürgens, H. W. & Ziegelmayer, G. *In Anthropologie. Handbuch Der Vergleichenden Biologie Des Menschen*Vol. 1 (Gustav Fischer, 1988).
19. Veselka, B. et al. Micro-CT assessment of dental mineralization defects indicative of vitamin D deficiency in two 17th-19th century Dutch communities. *Am. J. Phys. Anthropol.* **169**, 122–131. https://doi.org/10.1002/ajpa.23819 (2019).
20. D'Ortenzio, L., Kahlon, B., Peacock, T., Salahuddin, H. & Brickley, M. The rachitic tooth: Refining the use of interglobular dentine in diagnosing vitamin D deficiency. *Int. J. Paleopathol.* **22**, 101–108. https://doi.org/10.1016/j.ijpp.2018.07.001 (2018).
21. Kuremoto, K., Okawa, R., Matayoshi, S., Kokomoto, K. & Nakano, K. Estimation of dental age based on the developmental stages of permanent teeth in Japanese children and adolescents. *Sci. Rep.* **12**, 3345. https://doi.org/10.1038/s41598-022-07304-2 (2022).
22. Karadayı, B., Afşin, H., Ozaslan, A. & Karadayı, S. Development of dental charts according to tooth development and eruption for Turkish children and young adults. *Imaging Sci. Dent.* **44**, 103–113. https://doi.org/10.5624/isd.2014.44.2.103 (2014).
23. Tuteja, M., Bahirwani, S. & Balaji, P. An evaluation of third molar eruption for assessment of chronologic age: A panoramic study. *J. Forensic Dent. Sci.* **4**, 13–18. https://doi.org/10.4103/0975-1475.99154 (2012).
24. Akhlaghi, M. et al. Age-at-death estimation based on the macroscopic examination of Spheno-occipital sutures. *J. Forensic Leg. Med.* **17**, 304–308. https://doi.org/10.1016/j.jflm.2010.04.009 (2010).
25. Sahni, D., Jit, I. & Suri, S. Time of fusion of the basisphenoid with the basilar part of the occipital bone in northwest Indian subjects. *Forensic Sci. Int.* **98**, 41–45. https://doi.org/10.1016/S0379-0738(98)00135-2 (1998).
26. Mann, S. S., Naidich, T. P., Towbin, R. B. & Doundoulakis, S. H. Imaging of postnatal maturation of the skull base. *Neuroimaging Clin. N. Am.* **10**, 1–21 (2000).
27. Okamoto, K., Ito, J., Tokiguchi, S. & Furusawa, T. High-resolution CT findings in the development of the sphenooccipital synchondrosis. *Am. J. Neuroradiol.* **17**, 117–120 (1996).
28. Krishan, K. & Kanchan, T. Evaluation of spheno-occipital synchondrosis: A review of literature and considerations from forensic anthropologic point of view. *J. Forensic Dent. Sci.* **5**, 72–76. https://doi.org/10.4103/0975-1475.119764 (2013).
29. Higham, T. F. G., Jacobi, R. M. & Bronk Ramsey, C. AMS radiocarbon dating of ancient bone using ultrafiltration. *Radiocarbon* **48**(2), 179–195. https://doi.org/10.1017/S0033822200066388 (2006).
30. Brock, F., Higham, T. F. G. & Ditchfield, P. Current pretreatment methods for AMS radiocarbon dating at the oxford radiocarbon accelerator unit (ORAU). *Radiocarbon* **52**(1), 103–112. https://doi.org/10.1017/S0033822200045069 (2010).
31. Santos, G. M. et al. AMS 14 C sample preparation at the KCCAMS/UCI Facility: status report and performance of small samples. *Radiocarbon*(2), 255–269. https://doi.org/10.1017/S0033822200042181 (2007). 49.
32. Beverly, R. K. et al. The keck carbon cycle AMS laboratory, University of California, Irvine: Status report. *Radiocarbon*(2), 301–309. https://doi.org/10.1017/S0033822200045343 (2010). 52.
33. Reimer, P. J. & Reimer, R. W. A Marine reservoir correction database and on-line interface. *Radiocarbon* **43**(2A), 461–463. https://doi.org/10.1017/S0033822200038339 (2001).

34. Boaretto, E., Mienis, H. K. & Sivan, D. Reservoir age based on pre-bomb shells from the intertidal zone along the coast of Israel. *Nuclear Instrum. Methods Phys. Res. B.* **268**, 966–968. https://doi.org/10.1016/j.nimb.2009.10.075 (2010).
35. Renaud, G., Slon, V., Duggan, A. T. & Kelso, J. Schmutzi: estimation of contamination and endogenous mitochondrial consensus calling for ancient DNA. *Genome Biol.* **16**, 224. https://doi.org/10.1186/s13059-015-0776-0 (2015).
36. Ralf, A., González, D. M., Zhong, K., Kayser, M. & Yleaf Software for human Y-Chromosomal haplogroup inference from next-generation sequencing data. *Mol. Biol. Evol.* **35**, 1820. https://doi.org/10.1093/molbev/msy080 (2018).
37. Fernandes, D. M., Cheronet, O., Gelabert, P. & Pinhasi, R. TKGWV2: An ancient DNA relatedness pipeline for ultra-low coverage whole genome shotgun data. *Sci. Rep.* **11**, 21262. https://doi.org/10.1038/s41598-021-00581-3 (2021).
38. Alaçamlı, E. et al. READv2: Advanced and user-friendly detection of biological relatedness in archaeogenomics. *Genome Biol.* **25**, 216. https://doi.org/10.1186/s13059-024-03350-3 (2024).
39. Mittnik, A. et al. Kinship-based social inequality in Bronze Age Europe. *Science* **366**, 731–734. https://doi.org/10.1126/science.aax6219 (2019).
40. Agranat-Tamir, L. et al. The genomic history of the bronze age southern levant. *Cell* **181**, 1146–1157e11. https://doi.org/10.1016/j.cell.2020.04.024 (2020).
41. Posth, C. et al. The origin and legacy of the etruscans through a 2000-year archeogenomic time transect. *Sci. Adv.* **7**, eabi7673. https://doi.org/10.1126/sciadv.abi7673 (2021).
42. Matisoo-Smith, E. et al. Ancient mitogenomes of phoenicians from Sardinia and Lebanon: A story of settlement, integration, and female mobility. *PLoS One.* **13**, e0190169. https://doi.org/10.1371/journal.pone.0190169 (2018).
43. Moots, H. M. et al. A genetic history of continuity and mobility in the Iron Age central Mediterranean. *Nat. Ecol. Evol.* **7**, 1515–1524. https://doi.org/10.1038/s41559-023-02143-4 (2023).
44. Antonio, M. L. et al. Stable population structure in Europe since the Iron Age, despite high mobility. *eLife* 13, e79714 (2024). https://doi.org/10.7554/eLife.79714
45. Schmid, C. & Schiffels, S. Estimating human mobility in Holocene Western Eurasia with large-scale ancient genomic data. *Proc. Natl. Acad. Sci. USA*. 120, e2218375120 (2023). https://doi.org/10.1073/pnas.2218375120
46. Anastasiadou, K. et al. Detection of chromosomal aneuploidy in ancient genomes. *Commun. Biol.* **7**, 14. https://doi.org/10.1038/s42003-023-05642-z (2024).
47. Ringbauer, H., Novembre, J. & Steinrücken, M. Parental relatedness through time revealed by runs of homozygosity in ancient DNA. *Nat. Commun.* **12**, 1–11. https://doi.org/10.1038/s41467-021-25289-w (2021).
48. Carmichael, S. L. et al. Craniosynostosis and risk factors related to thyroid dysfunction. *Am. J. Med. Genet. A.* **167a**, 701–707. https://doi.org/10.1002/ajmg.a.36953 (2015).
49. Di Rocco, F. et al. Craniosynostosis and metabolic bone disorder. A review. *Neurochirurgie* **65**, 258–263. https://doi.org/10.1016/j.neuchi.2019.09.008 (2019).
50. Beaumont, J., Gledhill, A., Lee-Thorp, J., Montgomery, J. & Childhood Diet A closer examination of the evidence from Dental tissues using stable isotope analysis of Incremental Human Dentine. *Archaeometry* **55**, 277. https://doi.org/10.1111/j.1475-4754.2012.00682.x (2013).
51. Hillson, S. *Dental Anthropology* (Cambridge University Press, 1996).
52. Cobb, A. R. et al. The surgical management of treacher collins syndrome. *Br. J. Oral Maxillofac. Surg.* **52**, 581–589. https://doi.org/10.1016/j.bjoms.2014.02.007 (2014).
53. Weber, G. W. & Bookstein, F. L. Virtual Anthropology - A Guide to A New Interdisciplinary Field. (Springer Verlag. ISBN 978-3-211-48647-4, (2011).
54. Bastir, M. et al. Effects of brain and facial size on basicranial form in human and primate evolution. *J. Hum. Evol.* **58**, 424–431. https://doi.org/10.1016/j.jhevol.2010.03.001 (2010).
55. Bronk Ramsey, C. Bayesian analysis of radiocarbon dates. *Radiocarbon* **51**, 337–360. https://doi.org/10.1017/S0033822200033865 (2009).
56. Reimer, P. J. et al. IntCal13 and MARINE13 radiocarbon age calibration curves 0-50000 years calBP. *Radiocarbon* **55**(4), 1869–1887. https://doi.org/10.2458/azu_js_rc.55.16947 (2013).
57. Crann, C. A. et al. First status report on radiocarbon sample preparation at the A.E. Lalonde AMS Laboratory (Ottawa, Canada). *Radiocarbon* **59**, 695–704. https://doi.org/10.1017/RDC.2016.55 (2016).
58. Sirak, K. A. et al. A minimally-invasive method for sampling human petrous bones from the cranial base for ancient DNA analysis. *Biotechniques* **62**, 283–289. https://doi.org/10.2144/000114558 (2017).
59. Dabney, J. et al. Complete mitochondrial genome sequence of a middle pleistocene cave bear reconstructed from ultrashort DNA fragments. *Proc. Natl. Acad. Sci. USA*. **110**, 15758–15763. https://doi.org/10.1073/pnas.1314445110 (2013).
60. Korlević, P. et al. Reducing microbial and human contamination in DNA extractions from ancient bones and teeth. *Biotechniques* **59**, 87–93. https://doi.org/10.2144/000114320 (2015).
61. Meyer, M. & Kircher, M. Illumina sequencing library preparation for highly multiplexed target capture and sequencing. *Cold Spring Harb. Protoc.* db.prot5448 (2010). (2010). https://doi.org/10.1101/pdb.prot5448
62. Martin, M. Cutadapt removes adapter sequences from high-throughput sequencing reads. *EMBnet J.* **17**, 10–12. https://doi.org/10.14806/ej.17.1.200 (2011).
63. Li, H. & Durbin, R. Fast and accurate short read alignment with Burrows–Wheeler transform. *Bioinformatics* **25**, 1754–1760. https://doi.org/10.1093/bioinformatics/btp324 (2009).
64. Li, H. The Sequence Alignment/Map format and SAMtools. *Bioinformatics* **25**, 2078–2079. https://doi.org/10.1093/bioinformatics/btp352 (2009). Handsaker et al.1000 Genome Project Data Processing Subgroup.
65. Jónsson, H., Ginolhac, A., Schubert, M., Johnson, P. L. F. & Orlando, L. mapDamage2.0: Fast approximate bayesian estimates of ancient DNA damage parameters. *Bioinformatics* **29**, 1682–1684. https://doi.org/10.1093/bioinformatics/btt193 (2013).
66. Huang, Y. & Ringbauer, H. hapCon: estimating contamination of ancient genomes by copying from reference haplotypes. *Bioinformatics* **38**, 3768–3777. https://doi.org/10.1093/bioinformatics/btac390 (2022).
67. Jun, G., Wing, M. K., Abecasis, G. R. & Kang, H. M. An efficient and scalable analysis framework for variant extraction and refinement from population-scale DNA sequence data. *Genome Res.* **25**, 918–925. https://doi.org/10.1101/gr.176552.114 (2015).
68. Schönherr, S., Weissensteiner, H., Kronenberg, F. & Forer, L. Haplogrep 3 - an interactive haplogroup classification and analysis platform. *Nucleic Acids Res.* **51**, W263–W268. https://doi.org/10.1093/nar/gkad284 (2023).
69. Patterson, N. et al. Ancient admixture in human history. *Genetics* **192**, 1065–1093. https://doi.org/10.1534/genetics.112.145037 (2012).
70. Allentoft, M. E. et al. Population genomics of bronze age Eurasia. *Nature* **522**, 167–172. https://doi.org/10.1038/nature14507 (2015).
71. Antonio, M. L. et al. Ancient Rome: A genetic crossroads of Europe and the Mediterranean. *Science* **366**, 708–714. https://doi.org/10.1126/science.aay6826 (2019).
72. De Angelis, F. et al. First glimpse into the genomic characterization of people from the Imperial Roman Community of Casal Bertone (Rome, First-Third centuries AD). *Genes* **13**, 136. https://doi.org/10.3390/genes13010136 (2022).
73. de Damgaard, B. The first horse herders and the impact of early bronze age steppe expansions into Asia. *Science* **360**, eaar7711. https://doi.org/10.1126/science.aar7711 (2018).
74. Feldman, M. et al. Ancient DNA sheds light on the genetic origins of early Iron age Philistines. *Sci. Adv.* **5**, eaax0061. https://doi.org/10.1126/sciadv.aax0061 (2019).

75. Fernandes, D. M. et al. The spread of steppe and iranian-related ancestry in the islands of the western Mediterranean. *Nat. Ecol. Evol.* **4**, 334–345. https://doi.org/10.1038/s41559-020-1102-0 (2020).
76. Furtwängler, A. et al. Comparison of target enrichment strategies for ancient pathogen DNA. *Biotechniques* **69**, 455–459. https://doi.org/10.2144/btn-2020-0100 (2020).
77. Haber, M. et al. A genetic history of the Near East from an aDNA time course sampling eight points in the past 4,000 years. *Am. J. Hum. Genet.* **107**, 149–157. https://doi.org/10.1016/j.ajhg.2020.05.008 (2020).
78. Järve, M. et al. Shifts in the genetic landscape of the Western Eurasian Steppe associated with the beginning and end of the scythian dominance. *Curr. Biol.* **29**, 2430–2441e10. https://doi.org/10.1016/j.cub.2019.06.019 (2019).
79. Jones, E. R. et al. Upper palaeolithic genomes reveal deep roots of modern eurasians. *Nat. Commun.* **6**, 8912. https://doi.org/10.1038/ncomms9912 (2015).
80. Krzewińska, M. et al. Ancient genomes suggest the eastern Pontic-Caspian steppe as the source of western Iron age nomads. *Sci. Adv.* **4**, eaat4457. https://doi.org/10.1126/sciadv.aat4457 (2018).
81. Lazaridis, I. et al. The genetic history of the Southern Arc: A bridge between West Asia and Europe. *Science* **377**, eabm4247. https://doi.org/10.1126/science.abm4247 (2022).
82. Lazaridis, I. et al. Genomic insights into the origin of farming in the ancient Near East. *Nature* **536**, 419–424. https://doi.org/10.1038/nature19310 (2016).
83. Lipson, M. et al. Parallel palaeogenomic transects reveal complex genetic history of early European farmers. *Nature* **551**, 368–372. https://doi.org/10.1038/nature24476 (2017).
84. Marcus, J. H. et al. Genetic history from the middle neolithic to present on the mediterranean island of Sardinia. *Nat. Commun.* **11**, 939. https://doi.org/10.1038/s41467-020-14523-6 (2020).
85. Martiniano, R. et al. Genomic signals of migration and continuity in Britain before the anglo-saxons. *Nat. Commun.* **7**, 10326. https://doi.org/10.1038/ncomms10326 (2016).
86. Mathieson, I. et al. The genomic history of southeastern Europe. *Nature* **555**, 197–203. https://doi.org/10.1038/nature25778 (2018).
87. Mittnik, A. et al. The genetic prehistory of the Baltic sea region. *Nat. Commun.* **9**, 442. https://doi.org/10.1038/s41467-018-02825-9 (2018).
88. Narasimhan, V. M. et al. The formation of human populations in South and central Asia. *Science* **365**, eaat7487. https://doi.org/10.1126/science.aat7487 (2019).
89. Olalde, I. et al. The Beaker phenomenon and the genomic transformation of northwest Europe. *Nature* **555**, 190–196. https://doi.org/10.1038/nature25738 (2018).
90. Olalde, I. et al. The genomic history of the Iberian Peninsula over the past 8000 years. *Science* **363**, 1230–1234. https://doi.org/10.1126/science.aav4040 (2019).
91. Papac, L. et al. Dynamic changes in genomic and social structures in third millennium BCE central Europe. *Sci. Adv.* **7**, eabi6941. https://doi.org/10.1126/sciadv.abi6941 (2021).
92. Patterson, N. et al. Large-scale migration into Britain during the middle to late bronze age. *Nature* **601**, 588–594. https://doi.org/10.1038/s41586-021-04287-4 (2021).
93. Rivollat, M. et al. Ancient genome-wide DNA from France highlights the complexity of interactions between mesolithic hunter-gatherers and neolithic farmers. *Sci. Adv.* **6**, eaaz5344. https://doi.org/10.1126/sciadv.aaz5344 (2020).
94. Seguin-Orlando, A. et al. Heterogeneous hunter-gatherer and steppe-related ancestries in late neolithic and bell beaker genomes from present-day France. *Curr. Biol.* **31**, 1072–1083e10. https://doi.org/10.1016/j.cub.2020.12.015 (2021).
95. Skourtanioti, E. et al. Genomic history of neolithic to bronze age anatolia, Northern Levant, and Southern Caucasus. *Cell* **181**, 1158–1175e28. https://doi.org/10.1016/j.cell.2020.04.044 (2020).
96. Zalloua, P. et al. Ancient DNA of phoenician remains indicates discontinuity in the settlement history of Ibiza. *Sci. Rep.* **8**, 17567. https://doi.org/10.1038/s41598-018-35667-y (2018).
97. Patterson, N., Price, A. L. & Reich, D. Population structure and eigenanalysis. *PLoS Genet.* **2**, e190. https://doi.org/10.1371/journal.pgen.0020190 (2006).
98. Mallick, S. et al. The Allen Ancient DNA resource (AADR) a curated compendium of ancient human genomes. *Sci. Data.* **11**, 182. https://doi.org/10.1038/s41597-024-03031-7 (2024).

Acknowledgements

We thank Ernst Rudolf and Peter Scherrer for their motivation to take up research on the Octagon cranium again. It had been published in 1953 already by the former head of our institute, but the new investigations using current knowledge and state-of-the-art technology brought surprising new facts to light. We are grateful to Martin Dockner for help with the µCT scanning of the cranium. We thank Gro Bjørnstad for taking the samples and the General Directorate for Cultural Heritage and Museums in Ankara for the opportunity to export the samples from the Octagon femur and rib. We thank Sabine Eggers, Karin Wiltschke-Schrotta, Eduard Winter, and Maria Teschler-Nicola (Natural History Museum, Vienna, Austria), and Israel Hershkovitz (Department of Anatomy and Anthropology, Sackler Faculty of Medicine, Tel Aviv University, Israel) for granting access to the comparable materials. This project was funded by the Research Network "Human Evolution and Archaeological Sciences (HEAS)", University of Vienna, No. 369300, and the University of Vienna Grant No. BE547005.

Author contributions

G.W.W. designed and coordinated the study and took all photographs of the cranium. P.G.Š. performed the image data processing, 3D surface acquisition and landmark collection. G.W.W and P.G.Š. examined the cranium, measured, analysed and interpreted morphological data, conducted GM analyses, and wrote the basic manuscript, O.C. and A.L.L. did the genetics lab work, P.G. designed the capture kit for the rib, D.F., O.C. and R.P. performed and interpreted the genetic analyses, K.S. and T.H. conducted the dating analysis, M.S., I.T. and S.L. worked on the archaeological interpretation of the findings, E.U. examined the teeth and worked on the interpretation of the tooth status and masticatory aspects, H.W. and K.M. identified the cranium in the collection of the Department of Evolutionary Anthropology, University of Vienna. All authors contributed to the final version of the manuscript.

Declarations

Competing interests

The authors declare no competing interests.

Additional information

Supplementary Information The online version contains supplementary material available at https://doi.org/10.1038/s41598-024-83870-x.

Correspondence and requests for materials should be addressed to G.W.W.

Reprints and permissions information is available at www.nature.com/reprints.

Publisher's note Springer Nature remains neutral with regard to jurisdictional claims in published maps and institutional affiliations.